# Preliminary design of the inlet duct of a dust analyzer for Mars

Gianandrea Vittorio Messa[1], Stefano Malavasi[1] , Diego Scaccabarozzi[2] , Bortolino Saggin[2], Marco Tarabini[2], Francesca Esposito[3], Cesare Molfese[3]

1 Department of Civil and Environmental Engineering
Politecnico di Milano
Milan, Italy
2 Department of Mechanical Engineering
Politecnico di Milano
Milan, Italy
3 INAF - Osservatorio Astronomico di Capodimonte,
Naples, Italy
diego.scaccabarozzi@polimi.it

***Abstract*— Airborne dust characterization is very important in planetary climatology, especially on Mars, where dust is always present and its concentration varies with seasons. This work deals with the design of the inlet duct of an instrument named MicroMED, devoted to characterize Martian dust but suitable to be mounted on different planetary landers or rovers. An inertial classifier has been developed to cut particles with diameter larger than 20 µm in order to avoid obstruction of the pumping system of the instrument. CFD simulations based on the Eulerian-Lagrangian approach were performed to characterize the separation performance of the classifier. Finally, the inlet duct has been mechanically designed by FE approach to assure resistance and proper mechanical behavior within expected mechanical environment.**

***Keywords—MIcroMED instrument; ExoMars 2018 mission, Inertial Filter, CFD, Two phase flow.***

## I. INTRODUCTION

MicroMED is an optical particle counter able to measure the size distribution and density of dust particles suspended into Martian atmosphere. The instrument has been proposed as a European contribution to the Russian-led Instrument "Dust Suite" [1]. It is a lighter and simplified version of the instrument MEDUSA [2,3], previously selected by ESA for being accommodated on the Humboldt payload of the ExoMars mission. MicroMED is able to measure the dust size distribution and abundance versus size in the range from 0.2 to 20 µm in equivalent radius, analyzing light scattered from single dust particles. The working principle is provided in Fig. 1. A specially designed pump [4] is used to sample the Martian atmosphere, generating a flux of gas and dust across the instrument trough the inlet. When the dust grains reach the optical sensor head, cross a collimated laser beam emitted by a laser diode. The light scattered by the grains is detected by a photodiode whose signal is amplified and processed by the main electronics. The detected signal is related to the size of sampled dust particle. Preliminary testing performed on an elegant breadboard in simulated Martian environment [3] demonstrated functionality of the instrument, providing a TRL between 5 and 6. The MicroMED breadboard is shown in Fig. 2. Beside the pump, the inlet duct is critical for the intended application. In fact, this component shall be designed to achieve a uniform velocity field of the particles in the optical head sampling volume and prevent coarse particles from entering the sampling flux.

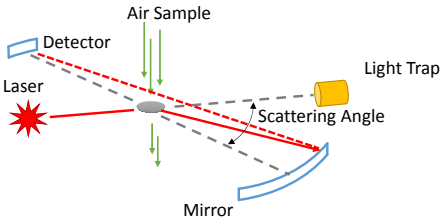


Fig. 1. Optical measurement principle of MicroMED.

Large particles can obstruct the inlet duct or even the pumping system, causing mission failure. Thus, a proper filter has been designed in order to cutout particles with diameter greater that about 20 µm, largest size of interest for the instrument scientific objectives. The work undertaken for the preliminary design of the filter is described in this paper. Particularly, CFD analyses were first performed to characterize the filter from the point of view of its separation efficiency. Afterwards, FE simulations were run to achieve mass and size minimization.

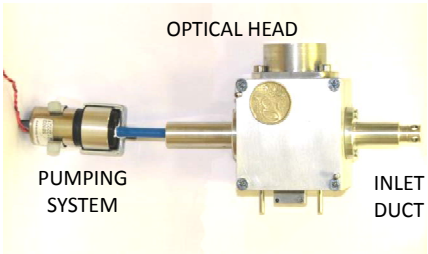


Fig. 2. MicroMED breadboard.

## II. PRELIMINARY DESIGN CONSIDERATIONS

### A. Types of inertial classifiers

In order to remove the bigger particles from the gas stream, their inertia has been exploited, thereby making use of an inertial classifier. The functioning of such devices relies on the fact that, if the gas flow is curved, particles with sufficient large inertia escape the flow whereas the others stay within the gas streamlines. There are four types of inertial classifiers, i.e. the body, conventional, virtual impactors and the cyclone (Fig. 3).

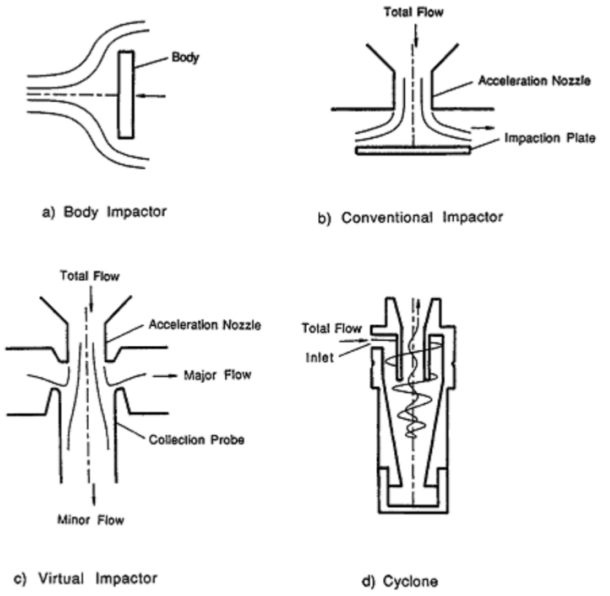


Fig. 3. Four types of inertial classifiers (picture taken from [5]).

The body impactor is a body in a moving aerosol stream onto which particles impact, whereas the conventional impactor (in its simplest form) consists of a jet of particle-laden gas impinging on a flat plate. The virtual impactor classifier is a collection probe slightly larger than the nozzle. A small fraction of the particles passes through the collection probe allowing classification of the particles. Finally, in a cyclone the aerosol stream is drawn through the inlet and it impinges tangentially on the inner surface of the cylinder generating a spiral pattern. Conical element inside the cyclone reverses the flow and, due to the inertial properties of the particles, it allows dust classification. Preliminary comparison among available solutions evidenced that the body impactor is the simplest and lightest system to filter dust particles; therefore, it has been selected for the present application. Particularly, the body consists of a sphere whose diameter was 6 mm to minimize located mass and size for the designed filter.

In order to establish the performance of impactors, reference is usually made to the curve of the impactor efficiency η versus the square root of the Stokes number [5]. The Stokes number of a body impactor is defined as

$$St = \frac{\rho_p C_c d_p^2 V_{rel}}{18 \mu d_b} \quad (1)$$

where $\rho_p$ is the particle density, $C_c$ is the Cunningham slip correction, $d_p$ is the particle diameter, $\mu$ is the gas viscosity, $d_b$ is the characteristic size of the body impactor (i.e. the diameter of the sphere in this case), and $V_{rel}$ is the relative average velocity between the body and the gas flow. The impactor efficiency $\eta$ is given as the ratio between the number of particles with given Stokes number that are impacted on the sphere from a volume of air swept out by the body. At the preliminary design stage, emphasis is upon the value of $St$ corresponding to a 50% efficiency, referred to as $St_{50}$. The particle size associated to $St_{50}$ is referred to as $d_{p,50}$.

### B. Fluid-dynamic charcterization of the Martian atmosphere

The Martian atmosphere has been regarded as a mixture of a gas and solid particles (the dust). The fluid-dynamic properties of the two phases that have been considered in this study are as follows.

The gas has density and viscosity equal to 0.02 kg/m$^3$ and $1.5 \cdot 10^{-5}$ Pa·s, respectively, and the characteristic wind speed one meter high from the Mars surface was taken as 7.5 m/s. According to [6], the maximum mass loading in a dust storm, i.e. the ratio between the mass of the particles and that of the gas, is 4.5 $10^{-4}$, whilst in average conditions the maximum mass loading is 2.2 $10^{-5}$ and the mean is 1.06 $10^{-5}$. In the simulations, reference was made to the latter value. During a dust storm, the sources of particulate are the atmosphere, from where small particles slowly settle out while being mixed with the boundary layer by turbulence, and the planet surface, from which coarser particles lifted off after deposition come. Taylor et al. [7] reported the particle size distribution of the two groups of particles one meter high from the Mars surface. These results helped in defining the characteristics of the particulate phase considered in this study; particularly, the small and the coarse particles have peak diameters of 1.6 μm and 50 μm, respectively. The particle density was taken as 2730 kg/m$^3$.

## III. FLUID-DYNAMIC MODELLING

### A. Gas-particle two-phase model

The gas-particle flow was simulated by means of the Eulerian-Lagrangian model embedded in the Ansys Fluent CFD code version 15.0. In the Eulerian-Lagrangian approach, the gas phase is considered a continuous mean, whilst the solid phase is simulated by following the trajectories of parcels, i.e. groups of particles sharing the same fluid dynamic properties [8]. The low particle mass loading considered in this study, that is that characteristic of the average condition in the Martian atmosphere (1.06 $10^{-5}$), enables the hypothesis of one-way coupling regime, i.e. the assumption that the gas affects the motion of the particles but not vice-versa [9]. Therefore, the gas flow without particles was first simulated by solving the RANS equations in conjunction with the $k$-ε realizable turbulence model for evaluation of the Reynolds stress tensor [10]. Afterwards, the trajectories of each parcel are evaluated by solving the following set of ODEs:

$$\begin{cases} \dfrac{d\mathbf{x}}{dt} = \mathbf{v} \\ \dfrac{d\mathbf{v}_p}{dt} = \dfrac{3}{4d_p}\dfrac{\rho_f}{\rho_p} C_d \left|\mathbf{u}^* - \mathbf{v}\right| \left(\mathbf{u}^* - \mathbf{v}\right) \end{cases} \quad (2)$$

in which **x** and **v** are the parcel's position and instantaneous velocity vectors, respectively; $\rho_f$ is the density of the gas; $C_d$ is the drag coefficient; and **u*** is the instantaneous gas velocity at the parcel's position. The drag coefficient is obtained by the well-known correlation of Shiller and Naumann [11].

$$C_d = \max\left[\frac{24}{\mathrm{Re}_p}\left(1 + 0.15\,\mathrm{Re}_p^{0.687}\right), 0.44\right] \quad (3)$$

where $\mathrm{Re}_p = \rho_f |\mathbf{u}^* - \mathbf{v}| / \mu$ is the particle Reynolds number. Due to the high gas-to-particle density ratio, turbulent dispersion and forces other than the form drag were neglected, being apparently related to side effects of minor importance for the case study under consideration.

### *B. Computational domain and boundary conditions*

The computational domain, sketched in Fig. 4, consists of a half cylinder with diameter of 350 mm and height of 800 mm. In the middle of the domain, the designed impactor is placed.

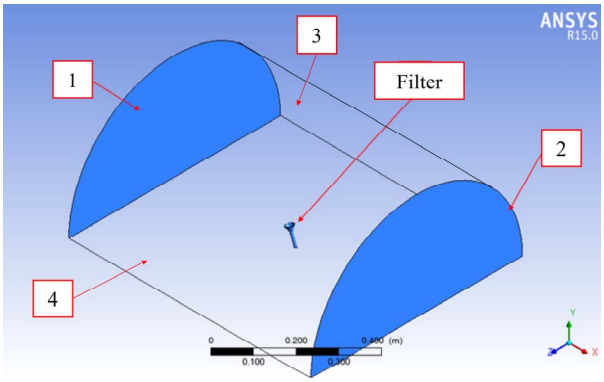


(a)

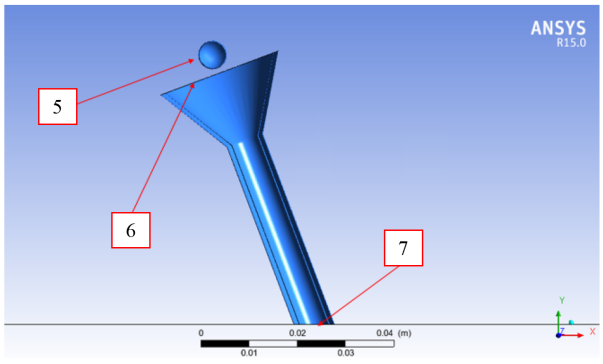


(b)

Fig. 4. Sketch of the computational domain: (a) overall view (b) detailed view of the filter

TABLE I. BOUNDARY CONDITIONS FOR GAS PHASE AND PARCELS

| Face | Gas phase | Parcels |
|---|---|---|
| 1 | Imposed velocity, k and ε | Imposed position and velocity |
| 2 | Fixed pressure | Escape |
| 3 | Fixed pressure | Escape |
| 4 | No slip, equ. wall function | Reflect |
| 5 | No slip, equ. wall function | Stick |
| 6 | No slip, equ. wall function | Reflect |
| 7 | Imposed velocity, k, and ε | Escape |

The boundary conditions applied to the fluid and to each parcel are summarized in Table 1 for all domain faces. The gas phase enters the domain through face 1 with velocity of 7.5 m/s normal to the boundary, and it leaves through faces 2, 3 (where a 0 relative pressure is imposed) and 7 (where an outward-directed velocity of 4 m/s normal to the boundary is imposed). The turbulent kinetic energy *k* and its dissipation rate ε on faces 1 and 7 are obtained from a turbulent intensity of 10% and turbulent length scales of 350 mm and 5 mm, respectively. A no slip condition is imposed to the gas phase on all solid walls (faces 4 to 6), and the standard wall function [12] is employed for modelling the wall shear stress and the values of *k* and ε in the near-wall cells. The particles are injected in the domain through face 1, with velocity equal to that of the fluid, and they can escape through faces 2, 3, and 7. The particles hitting the spherical body (face 5) remain stuck to the wall, and the calculation of their trajectories is stopped. The particles hitting all the other solid surfaces (faces 4 and 6) bounce with unit restitution coefficients.

Two parcels' injections are defined on face 2, one for each of the two particle groups described in Section II.B. For each group, the initial position of the parcels are randomly extracted from a uniform distribution, whilst the particle sizes are obtained by fitting the results of Taylor *et al.* [7] to a Rosin-Rammler distribution. The number of injected parcels was changed, and the mass flow rate of each parcel was varied accordingly to keep the total solid mass loading constant and equal to $1.06\ 10^{-5}$.

### *C. Computational methodology and consistency of the numerical solution*

The impactor efficiency was calculated as the ratio between the number of parcels of a given size that remain stuck on the sphere (face 5) and the number of injected parcels having the same size. This value has been calculated for different particle sizes, which have been associated to the corresponding Stokes numbers. This is done by applying Eq. (1) with $V_{rel}$ = 7.5 m/s and $C_c \approx 1$. The curve of efficiency versus the square root of Stokes number was determined and, finally, $\sqrt{St}_{50}$ and $d_{p,50}$ have been found by a trial-error procedure.

In order to guarantee the reliability of the obtained estimates, sensitivity analyses upon the effect of mesh discretization and the number of injected parcels were performed. Particularly,

three different meshes consisting of about $3 \cdot 10^5$, $6 \cdot 10^5$, and $1.3 \cdot 10^6$ were employed, and the GCI method of Roache [13] was applied to quantify the grid discretization error on the finer mesh. The GCI of $\sqrt{St_{50}}$ was 1.03%, thereby proving the suitability of the used grid. In the same way, the number of injected parcels was increased from about $2.5 \cdot 10^4$ up to about $7.5 \cdot 10^4$ and the influence of such variation upon the impactor efficiency corresponding to a particle size of 22 µm was studied. The results, shown in Fig. 5, indicate that the impactor efficiency tends to approach a constant value of about 50-52% as the number of parcels is increased. The estimate obtained with $7.5 \cdot 10^4$ parcels was judged satisfactory for this preliminary study.

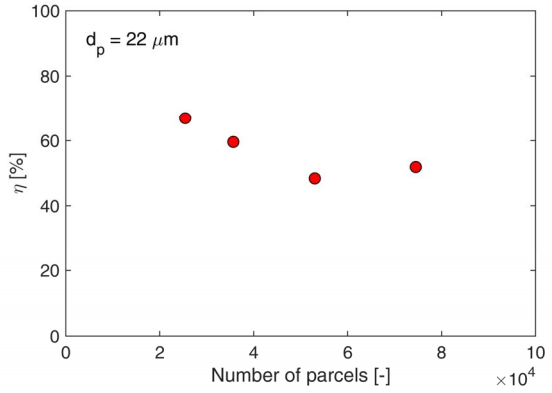


Fig. 5. Sensitivity of the impactor efficiency for a particle size of 22 µm with respect to the number of injected parcels.

### D. Results and discussion

The objective of the CFD analyses was essentially to determine the trend of the impactor efficiency, $\eta$, versus the square root of Stokes number, $\sqrt{St}$. As it has been already remarked, this curve is an important technical parameter of body impactors, which allows establishing their separation performance. The obtained curve is shown in Fig. 6; the data indicate that the value of $\sqrt{St}$ corresponding to a 50% impactor efficiency, $\sqrt{St_{50}}$, is around 2.25. This gives, in turn, a $d_{p,50}$ around 22 µm.

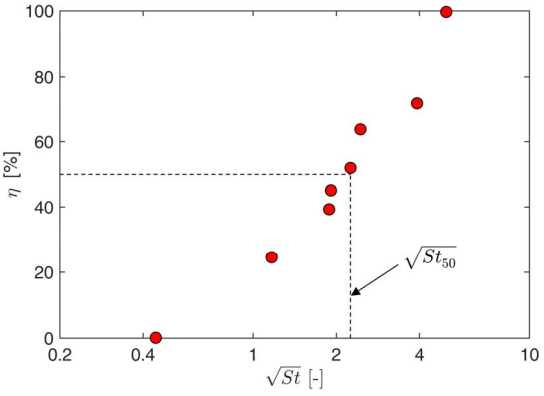


Fig. 6. Impactor efficiency as a function of the square root of the Stokes number. The value of $\sqrt{St_{50}}$, corresponding to a particle size of about 22 µm, is highlighted too.

The CFD simulations indicate that the designed impactor is suitable for its purpose in the considered flow conditions. Anyway, emphasis is upon the preliminary nature of this study, which must be necessarily followed by further fluid dynamic analyses. First, it is important to notice that all the design was done in average condition of the Martian atmosphere and that the filter efficiency shall be measured in the extreme conditions of Mars (e.g. dust storms). Afterwards, optimization of the circuit should be done to reduce as much as possible the pressure losses of the pipeline.

## IV. MECHANICAL DESIGN

### A. Design Requirements

Thermo-mechanical design of the MicroMED is driven by the following requirements:

- a quasi-static design load of about 500 m/s$^2$ has to be overcome;
- a first natural frequency above 130 Hz shall be provided to avoid coupling with lower frequency satellite modes;
- sweep sine vibration between 20 and 100 Hz with acceleration amplitude of 240 m/ s$^2$,
- random excitation between 20 and 2000 Hz with PSD amplitude up to 0.102 g$^2$/Hz.

Overall mass to of the instrument is about 0.5 kg including electronics (about 150g) and the design contingency (20%). Moreover, thermal environment requires storage between -50 and 40°C and working temperature range between -20 and 40°C. Thus, for the mechanical design of the filter/inlet part minimization of the located mass and size was mandatory.

### B. FE Analyses

Inertial filter design was performed with the following FE analyses:

- Quasi-static analyses under design load; and
- Buckling analyses under quasi-static loading; and
- Modal analyses to verify mechanical behavior of the filter.

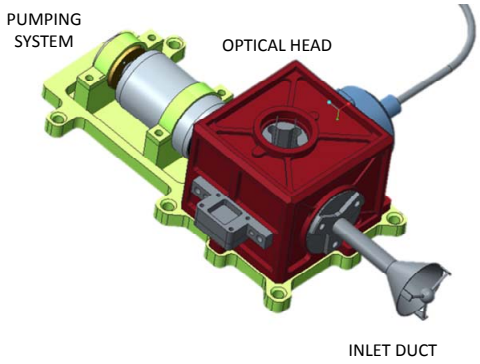


Fig. 7. MicroMED 3D model.

In order to achieve mass minimization, two different configurations were investigated. The thickness of the inlet duct was set to 0.5 and 0.25 mm. The latter was considered as manufacturing limit with conventional technology. Al7075T6 alloy was selected as baseline for the inlet duct design. A FE model of the duct was developed. The filter was constrained near the connection with the optical stage, shown in Fig. 7, where sketch of the MicroMED 3D model is provided. Simulation results are summarized in Table II. Figures 8 and 9 describe computed Von Mises stress and filter dynamic behavior for the lowest thickness.

TABLE II. RESULTS OF THE MODAL, QUASI-STATIC AND BUCKLING ANALYSES.

| Thickness [mm] | 1st Mode [Hz] | 2nd Mode [Hz] | 3rd Mode [Hz] | Von Mises Stress [MPa] | BF | Mass [g] |
|---|---|---|---|---|---|---|
| 0.25 | 1029 | 1030 | 2120 | 16.1 | 483 | 4.8 |
| 0.5 | 1321 | 1322 | 2838 | 11.2 | 1806 | 5.9 |


Fig. 8. Von Mises stresses, case study 0.25mm, quasi-static analysis.

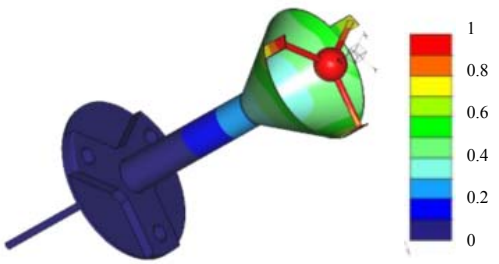


Fig. 9. Adimensional displacement, Modal analysis, case study 0.25mm, frequency 1029 Hz.

### C. Discussion

FE analyses evidenced that both the analyzed configurations satisfy the resistance requirements providing a large margin of safety against yield. A very low Von Mises stress is achieved near the connection of the inertial filter, about 16 MPa. Similar conclusion can be stated for the buckling analyses and the computed dynamic behavior. In fact, both the BF and the first natural frequency are very far from the acceptable limits, i.e. 3 and 130 Hz. For what concern the mass budget, both the solutions are fully acceptable, thanks to a computed mass of about 1% of the overall instrument mass budget.

## V. CONCLUSIONS

This study is part of a research aimed at developing a space instrument devoted to dust analysis in Martian environment. Particularly, this work aims at preliminary designing the inlet duct of the system, which comprises a body impactor for preventing the coarser particles from entering the instrument optical stage. CFD simulations highlighted that, for the designed impactor, the particle size corresponding to a 50% filter efficiency is about 22 μm in the average atmospheric Martian conditions, thereby confirming the suitability of the impactor for its purpose. The obtained solution allows protection of the pumping system as well, assuring the instrument working for all the expected duration of the mission. Mechanical design of the filter was successfully assessed by finite element analyses simulating expected loading at the instrument launching and landing on Mars. The next steps of this research will consist of a proper CFD design of the optical stage, aimed at computing and verifying the instrument sampling efficiency, and a fluid-dynamic optimization of circuit should be done to reduce as much as possible the pressure losses. Moreover, some experimental activity is planned to validate the filter design.

## ACKNOWLEDGMENT

Authors would like to acknowledge Ivan Lopez for his contribution in this activity.

## REFERENCES

[1] Russian Academy of Sciences, Space Research Institute (IKI), 'ExoMars 2018 Surface Platform Experiment Proposal Information Package', 2015.

[2] Colangeli, L. *et al.*, "MEDUSA: The ExoMars experiment for in-situ monitoring of dust and water vapour", Planetary and Space Science, 2009, 57, (8–9), pp. 1043-1049.

[3] Esposito, F. *et al.* "MEDUSA: Observation of atmospheric dust and water vapor close to the surface of Mars", Mars 6, 2011, pp. 1-12.

[4] Scaccabarozzi, D., et al., 'Characterization of a pumpng system in Martian-like environment', IEEE Metrology for Aerospace, 2014, pp. 150-154.

[5] P. Kulkarni *et al.*, *Aerosol Measurement: Principles, Techniques, and Applications*, New York: Wiley, 2011.

[6] LMD/OU/IAA/ESA/CNES. Mars climate datatabase. http://wwwmars.lmd.jussieu.fr/mars/access.html, 5.2 Web Interface.

[7] P.A. Taylor *et al.*, "Modelling dust distributions in the atmospheric bounday layer on Mars", *Boundary-Layer Meteorol.,* vol. 125, pp. 305-328, 2007.

[8] C.T. Crowe *et al.*, "The Particle-Source-In Cell (PSI-CELL) Model for Gas-Droplet Flows", *ASME J Fluids Eng*, vol. 99, no. 2, pp. 325-332, 1977.

[9] E. Loth, "Numerical approaches for motion of dispersed particles, droplets, and bubbles", *Prog. En. Comb. Sci.* vol. 26, pp. 161-223, 2000.

[10] T.H. Zhih *et al.*, "A new eddy viscosity model for high Reynolds number turbulent flows – Model development and validation", *Comput. Fluids*, vol. 24, no. 3, pp. 227-238, 1995.

[11] L. Shiller and A. Naumann, "A drag coefficient correlation", *Z. Ver. Deutsch. Ing.* vol. 77, pp. 318-320, 1935.

[12] B.E. Launder and D.B. Spalding, "The numerical computation of turbulent flows", *Comput. Meth. Applied Mech. Eng.* vol. 3, pp. 269-289, 1974.

[13] P.J. Roache, "Perspective: a method for uniform reporting of grid refinement studies", *ASME J Fluids Eng*, vol. 116, no. 3, pp. 405-413, 1994.